Relative Impedance Control for Dual-Arm Robots Performing Asymmetric Bimanual Tasks

Jinoh Lee, *Member, IEEE*, Pyung Hun Chang, *Member, IEEE*, and Rodrigo S. Jamisola, Jr., *Member, IEEE*

***Abstract*—This paper presents a method of implementing impedance control (with inertia, damping, and stiffness terms) on a dual-arm system by using the relative Jacobian technique. The proposed method significantly simplifies the control implementation because the dual arm is treated as a single manipulator, whose end-effector motion is defined by the relative motion between the two end effectors. As a result, task description becomes simpler and more intuitive when specifying the desired impedance and the desired trajectories. This is the basis for the relative impedance control. In addition, the use of time-delay estimation enhances ease of implementation of our proposed method to a physical system, which would have been otherwise a very tedious and complicated process.**

***Index Terms*—Asymmetric bimanual task (ABT), dual arm, ideal-velocity feedback (IVF), impedance control, relative Jacobian, time-delay estimation (TDE).**

I. Introduction

DUAL-ARM robots provide a platform for implementing humanly intuitive tasks and, possibly, straightforwardly replace humans in performing some of their work. These tasks may involve high technology, e.g., outer-space assembly and repair, or domestic work, e.g., assisting the elderly in the household chores. The biggest challenge in dual arms, however, is the complexity of manipulation. Thus, it is advantageous to adopt a strategy to address this complexity and, at the same time, accommodate human intuitiveness in the task requirements.

This work presents a method of implementing impedance control on a dual-arm system that is controlled as a single manipulator. It allows an easier coordination of interaction between the two arms. This single controller was possible via a relative Jacobian [1], [2], which maps the joint velocities of the two arms to the relative motion between their end effectors, thus the name relative impedance control. The relative Jacobian is derived by combining the individual Jacobians of each arm. From the control perspective, it creates an effective single arm with kinematic redundancy, which contributes to the simplification of control strategy. The use of time-delay estimation (TDE) [3]–[6] further simplifies our implementation by estimating the robot dynamics from the imprecise dynamics information of the dual arm.

Dual arms are inherently designed to interact with each other and, in some cases, with their environment. Many studies on such interaction used impedance control [7]–[9] that is internal (between manipulators) [10]–[12] and/or external (between manipulator and environment) [10], [12]. In this paper, relative impedance control refers to impedance control that is expressed in relative reference frames, which can be internal or external.

Bimanual tasks can be classified as symmetric or asymmetric [13], [14]. In symmetric bimanual tasks, both arms play the same role: in an in-phase manner, e.g., lifting a single object with both arms [11], [12], [15]–[17], or in an out-of-phase manner, e.g., rope climbing [13]. In asymmetric bimanual tasks (ABTs), each arm performs a different role, but each is necessary to achieve a desired task, e.g., dealing cards [13], writing a handy note [18], part mating or assembly [19], [20], and opening a jar [21]. It has been experimentally shown that bimanual task coordination in humans activates a different part of the brain as compared to unimanual task movements [22], [23]. In this paper, the ABT is performed with the right hand writing a circle on a plate attached to the left hand. Recent studies on dual-arm/multiple robots include [24]–[26], and bioinspired robots and control strategies include [27]–[39].

The difference of our work compared to previous studies of impedance control on dual-arm systems is stated here. The work in [21] used two anthropomorphic dual arms of Justin to unscrew a can. It used impedance control without the inertia term and did not use a relative Jacobian. In [40], two six-degree-of-freedom (DOF) Kuka robots that held an egg used adaptive force/motion control and did not use a relative Jacobian. Coordination of n-cooperating manipulators was discussed in [11] with full impedance control but used no relative Jacobian. Full impedance control of two 6-DOF manipulators was shown in [12] but did not use a relative Jacobian. Two 2-DOF Selective Compliance Assembly Robot Arm (SCARA) robots with full impedance control were used in [10] but the did not use a relative Jacobian. SCARA and Programmable Universal Manipulation Arm (PUMA) 560 robots with full impedance control were used in [41], but no relative Jacobian was used. A previous study that is closest to our work is [42], which used impedance control with relative Jacobian. However, the impedance control

Manuscript received September 29, 2012; revised December 28, 2012 and March 18, 2013; accepted May 11, 2013. Date of publication June 4, 2013; date of current version January 31, 2014. This work was supported in part by the Ministry of Education, Science, and Technology of Korea through the Daegu Gyeongbuk Institute of Science and Technology R&D Program under Grant 11-BD-0402, and in part by the NRF-2013M2A2A 4023350.

J. Lee is with the Department of Advanced Robotics, Istituto Italiano di Tecnologia, 16163 Genoa, Italy (e-mail: jinoh.lee@iit.it).

P. H. Chang was with the Department of Mechanical Engineering, Korea Advanced Institute of Science and Technology, Daejeon 305-701, Korea. He is now with the Department of Robotics Engineering, Daegu Gyeongbuk Institute of Science and Technology, Daegu 711-873, Korea (e-mail: phchang@dgist.ac.kr).

R. S. Jamisola, Jr., is with the Department of Robotics Engineering, Daegu Gyeongbuk Institute of Science and Technology, Daegu 711-873, Korea (e-mail: rjamisolajr@dgist.ac.kr).

Color versions of one or more of the figures in this paper are available online at http://ieeexplore.ieee.org.

Digital Object Identifier 10.1109/TIE.2013.2266079

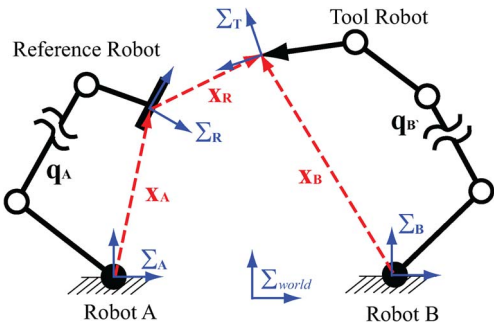

Fig. 1. Schematic diagram of a dual arm with robot A (reference robot) and robot B (tool robot). We used the following notation: $\mathbf{q}_A$—joint angles of robot A; $\mathbf{q}_B$—joint angles of robot B; $\mathbf{x}_R$—relative position and orientation vector with respect to $\mathbf{\Sigma}_R$; $\mathbf{\Sigma}_{\text{world}}$—world frame; $\mathbf{\Sigma}_A$—base frame of robot A; $\mathbf{\Sigma}_B$—base frame of robot B; $\mathbf{\Sigma}_R$—relative reference frame (located at robot A end effector); and $\mathbf{\Sigma}_T$—tool frame (located at robot B end effector). The position and orientation of robot A is $\mathbf{x}_A$, and for robot B, it is $\mathbf{x}_B$.

used was only a function of stiffness term, without inertia and damping terms. In addition, it did not use any cancellation of the dynamics of the system. There have been comparable dual-arm controls using disturbance observer, which is equivalent to TDE [43]. Studies in dual arms with disturbance observer and impedance control include [44]–[48]. However, all of these previous studies did not use relative Jacobian.

The contribution of this paper is on the proposition of relative impedance control for dual-arm systems to perform ABTs by simultaneously using relative Jacobian [1], [2] and TDE [3], [4] with ideal-velocity feedback (IVF) [49]. The use of relative Jacobian allows a simpler and more intuitive way of implementing impedance control (with inertia, damping, and stiffness terms) on a dual arm that is controlled as a single manipulator. Through our proposed method, only a single set of desired impedance and desired trajectories is used for the two end effectors. The use of TDE with IVF provides a convenient way of dynamics cancellation with minimal knowledge of the dynamics parameters of the dual arm.

This paper proceeds as follows. Section II presents the theoretical foundation of this work, which includes the relative impedance control formulation. Section III shows the description of our experimental setup and experimental results of a bimanual writing task. Section IV presents our conclusion. Finally, the Appendix discusses the stability analysis of our proposed controller.

II. Theoretical Foundations

The schematic diagram of our dual-arm robot performing ABT is shown in Fig. 1 with robot A as the reference robot and robot B as the tool robot. The reference frames are defined as follows: tool frame $\mathbf{\Sigma}_T$, located at robot B end effector; relative reference frame $\mathbf{\Sigma}_R$, located at robot A end effector; robot A base frame $\mathbf{\Sigma}_A$; robot B base frame $\mathbf{\Sigma}_B$; and world frame $\mathbf{\Sigma}_{\text{world}}$. The relative position and orientation vector $\mathbf{x}_R \in \mathbb{R}^{n_R}$ defines the position and orientation of $\mathbf{\Sigma}_T$ with respect to $\mathbf{\Sigma}_R$. The symbol n_R denotes the task space DOFs. Also shown in the figure are the position and orientation of robot A end effector, denoted as $\mathbf{x}_A$, and of robot B end effector, denoted as $\mathbf{x}_B$.

A. Relative Jacobian

Kinematically, the relative velocity vector $\dot{\mathbf{x}}_R \in \mathbb{R}^{n_R}$ is derived through the action of the relative Jacobian $\mathbf{J}_R \in \mathbb{R}^{n_R \times n_T}$ on the joint-space vector $\dot{\mathbf{q}} \in \mathbb{R}^{n_T} = [\dot{\mathbf{q}}_A^{\mathrm{T}} \quad \dot{\mathbf{q}}_B^{\mathrm{T}}]^{\mathrm{T}}$, i.e.,

$$\dot{\mathbf{x}}_R = \mathbf{J}_R \dot{\mathbf{q}}. \tag{1}$$

The symbols $\dot{\mathbf{q}}_A \in \mathbb{R}^{n_A}$ and $\dot{\mathbf{q}}_B \in \mathbb{R}^{n_B}$ represent the joint velocities of robots A and B, respectively, and $n_T = n_A + n_B$, where n_A and n_B are the DOFs of the respective robots. (From hereon, the subscripts A and B would refer to robots A and B, respectively.) This allows users to directly design the relative trajectory between the two end effectors so that implementing ABT becomes particularly simple. The expression of $\mathbf{J}_R$ can be derived from the individual Jacobians of each robot, i.e.,

$$\dot{\mathbf{x}}_R = \dot{\mathbf{x}}_B - \dot{\mathbf{x}}_A \tag{2}$$

such that

$$\dot{\mathbf{x}}_R = [\,-\mathbf{J}_A \quad \mathbf{J}_B\,]\,[\,\dot{\mathbf{q}}_A^{\mathrm{T}} \quad \dot{\mathbf{q}}_B^{\mathrm{T}}\,] \tag{3}$$

such that $\mathbf{J}_R = [-\mathbf{J}_A \quad \mathbf{J}_B]$ is the relative Jacobian with respect to the inertial reference frame. Similar to the aforementioned derivation is shown in [50]. However, in this paper, the expression of $\mathbf{J}_R$ used is the same as the expressions shown in [2] and [51].

B. Relative Impedance Control

The relative acceleration vector in the task space $\ddot{\mathbf{x}}_R$ can be expressed as $\ddot{\mathbf{x}}_R = \mathbf{J}_R \ddot{\mathbf{q}} + \dot{\mathbf{J}}_R \dot{\mathbf{q}}$, where $\dot{\mathbf{J}}_R$ denotes the derivative of $\mathbf{J}_R$ and $\ddot{\mathbf{q}}$ denotes the joint acceleration. The inverse kinematic solution is [52]

$$\ddot{\mathbf{q}} = \mathbf{J}_R^{+}\left(\ddot{\mathbf{x}}_R - \dot{\mathbf{J}}_R \dot{\mathbf{q}}\right) + \left(\mathbf{I} - \mathbf{J}_R^{+}\mathbf{J}_R\right)\boldsymbol{\nu} \tag{4}$$

where $\mathbf{I} \in \mathbb{R}^{n_T \times n_T}$ is an identity matrix and $\boldsymbol{\nu} \in \mathbb{R}^{n_T}$ is an arbitrary joint-space acceleration vector. In this paper, we use $\boldsymbol{\nu} = \mathbf{0}$, which means that the solution achieves the minimum norm acceleration.

The complete dynamics of the entire dual-arm system is expressed as a combined dynamics of robots A and B, i.e.,

$$\boldsymbol{\tau} = \mathbf{M}(\mathbf{q})\ddot{\mathbf{q}} + \mathbf{c}(\mathbf{q}, \dot{\mathbf{q}}) + \mathbf{g}(\mathbf{q}) + \mathbf{f}(\mathbf{q}, \dot{\mathbf{q}}) + \boldsymbol{\tau}_d + \boldsymbol{\tau}_e \tag{5}$$

where $\boldsymbol{\tau}_u = [\boldsymbol{\tau}_A^{\mathrm{T}} \quad \boldsymbol{\tau}_B^{\mathrm{T}}]^{\mathrm{T}} \in \mathbb{R}^{n_T}$ denotes the joint torque vector; $\mathbf{M}(\mathbf{q}) = \mathrm{diag}(\mathbf{M}_A(\mathbf{q}), \mathbf{M}_B(\mathbf{q})) \in \mathbb{R}^{n_T \times n_T}$ denotes the block diagonal of combined inertia matrices; $\mathbf{c}(\mathbf{q}, \dot{\mathbf{q}}) = [\mathbf{c}_A(\mathbf{q}, \dot{\mathbf{q}})^{\mathrm{T}}$ $\mathbf{c}_B(\mathbf{q}, \dot{\mathbf{q}})^{\mathrm{T}}]^{\mathrm{T}} \in \mathbb{R}^{n_T}$ denotes the combined torques of Coriolis and centrifugal forces; $\mathbf{g}(\mathbf{q}) = [\mathbf{g}_A(\mathbf{q})^{\mathrm{T}} \quad \mathbf{g}_B(\mathbf{q})^{\mathrm{T}}]^{\mathrm{T}} \in \mathbb{R}^{n_T}$ denotes the combined torques of gravitational forces; $\mathbf{f}(\mathbf{q}, \dot{\mathbf{q}}) = [\mathbf{f}_A(\mathbf{q}, \dot{\mathbf{q}})^{\mathrm{T}} \quad \mathbf{f}_B(\mathbf{q}, \dot{\mathbf{q}})^{\mathrm{T}}]^{\mathrm{T}} \in \mathbb{R}^{n_T}$ denotes the combined torques of Coulomb and viscous friction, and stiction; $\boldsymbol{\tau}_d \in \mathbb{R}^{n_T}$ denotes the torques due to disturbances; and $\boldsymbol{\tau}_e \in \mathbb{R}^{n_T}$ denotes the torques due to environmental contact forces.

The target dynamics of a physical system, such as the aforementioned equation, can be achieved through the desired impedance equation [7]–[9]. In this paper, we modify the desired impedance equation such that it can accommodate the relative motion between the two end effectors of the dual

arm, the internal impedance between them, and the (external) impedances for each end effector. The defined relationships are expressed in a formulation corresponding to an equivalent single manipulator

$$-\mathbf{f}_R = \mathbf{M}_{Rd}\left(\ddot{\mathbf{x}}_{Rd} - \ddot{\mathbf{x}}_R\right) + \mathbf{B}_{Rd}\left(\dot{\mathbf{x}}_{Rd} - \dot{\mathbf{x}}_R\right) + \mathbf{K}_{Rd}\left(\mathbf{x}_{Rd} - \mathbf{x}_R\right) \tag{6}$$

referenced at $\mathbf{\Sigma}_R$, where $\mathbf{f}_R \in \mathbb{R}^{n_R}$ denotes the relative contact forces between two end effectors, which can be obtained from the virtual work theorem [52] as $\boldsymbol{\tau}_e = \mathbf{J}_R^{\mathrm{T}}\mathbf{f}_R$; $\mathbf{M}_{Rd}$, $\mathbf{B}_{Rd}$, and $\mathbf{K}_{Rd} \in \mathbb{R}^{n_R \times n_R}$ denote the desired mass, damping, and stiffness matrices, respectively; and $\mathbf{x}_{Rd}$, $\dot{\mathbf{x}}_{Rd}$, and $\ddot{\mathbf{x}}_{Rd} \in \mathbb{R}^{n_R}$ denote the desired position and orientation, velocity, and acceleration vectors, respectively. The formulation (6) is called the *relative impedance control* equation, that allows a single control for the dual arm. As an example, when two 6-DOF robots are used in a dual-arm system, instead of managing 12 components to perform impedance control for the two arms, the proposed approach uses only six components for the equivalent single manipulator and is therefore easier to manage and implement. Furthermore, the desired motion is specified in terms of the relative motion between the end effectors with respect to the task frame.

C. TDE and IVF

There are two core techniques in this controller: TDE [3], [4] technique and IVF [49]. The TDE is an efficient and effective technique to estimate robot dynamics without a model. The IVF, which originated from natural admittance control [53], [54], is used for eliminating discontinuous nonlinearities such as Coulomb friction, stiction, and inertial force uncertainties. Note that the former takes care of continuous nonlinearity, whereas the latter takes care of discontinuous nonlinearity.

To eliminate the two nonlinearities of the system, we use TDE as follows. First, we re-express the robot dynamics as

$$\boldsymbol{\tau} = \bar{\mathbf{M}}\ddot{\mathbf{q}} + \mathbf{h}(\mathbf{q}, \dot{\mathbf{q}}, \ddot{\mathbf{q}}) \tag{7}$$

where $\bar{\mathbf{M}} \in \mathbb{R}^{n_T \times n_T}$ is a constant diagonal matrix, which may assume the nominal value of $\mathbf{M}(\mathbf{q})$, and $\mathbf{h}(\mathbf{q}, \dot{\mathbf{q}}, \ddot{\mathbf{q}}) = (\mathbf{M}(\mathbf{q}) - \bar{\mathbf{M}})\ddot{\mathbf{q}} + \mathbf{c}(\mathbf{q}, \dot{\mathbf{q}}) + \mathbf{g}(\mathbf{q}) + \mathbf{f}(\mathbf{q}, \dot{\mathbf{q}}) + \boldsymbol{\tau}_d + \boldsymbol{\tau}_e$.

Note that $\mathbf{h}(\mathbf{q}, \dot{\mathbf{q}}, \ddot{\mathbf{q}})$ contains all the continuous and discontinuous nonlinearities. In order to estimate it, we use TDE with the assumption that, for a given time t and a sampling period L that is sufficiently small, the following holds: $\lim_{L\to 0} \mathbf{h}(\mathbf{q}, \dot{\mathbf{q}}, \ddot{\mathbf{q}})_{(t-L)} = \mathbf{h}(\mathbf{q}, \dot{\mathbf{q}}, \ddot{\mathbf{q}})$. Let $\hat{\mathbf{h}}(\mathbf{q}, \dot{\mathbf{q}}, \ddot{\mathbf{q}})$ denote the estimate of $\mathbf{h}(\mathbf{q}, \dot{\mathbf{q}}, \ddot{\mathbf{q}})$; then, $\hat{\mathbf{h}}(\mathbf{q}, \dot{\mathbf{q}}, \ddot{\mathbf{q}}) = \mathbf{h}(\mathbf{q}, \dot{\mathbf{q}}, \ddot{\mathbf{q}})_{(t-L)}$. From (7), we obtain

$$\hat{\mathbf{h}}(\mathbf{q}, \dot{\mathbf{q}}, \ddot{\mathbf{q}}) = \boldsymbol{\tau}_{(t-L)} - \bar{\mathbf{M}}\ddot{\mathbf{q}}_{(t-L)}. \tag{8}$$

The robot dynamics in the operational space can be obtained by substituting (4)–(7), resulting in $\boldsymbol{\tau} = \bar{\mathbf{M}}\mathbf{J}_R^{+}(\ddot{\mathbf{x}}_R - \dot{\mathbf{J}}_R\dot{\mathbf{q}}) + \mathbf{h}(\mathbf{q}, \dot{\mathbf{q}}, \ddot{\mathbf{q}})$, where, from (4), we set $\boldsymbol{\nu}$ to zero. From (7), we set $\boldsymbol{\tau} = \boldsymbol{\tau}_u$, where $\boldsymbol{\tau}_u$ is the control torque which is designed as follows:

$$\boldsymbol{\tau}_u = \bar{\mathbf{M}}\mathbf{J}_R^{+}\left(\mathbf{v}_d - \dot{\mathbf{J}}_R\dot{q}\right) + \hat{\mathbf{h}}(\mathbf{q}, \dot{\mathbf{q}}, \ddot{\mathbf{q}}). \tag{9}$$

The symbol $\mathbf{v}_d$ is a control law that combines the relative impedance equation with the IVF correction term and is expressed as

$$\mathbf{v}_d = \underbrace{\ddot{\mathbf{x}}_{Rd} + \mathbf{M}_{Rd}^{-1}\left(\dot{x}_{Rd} - \dot{x}_R\right) + \mathbf{K}_{Rd}(\mathbf{x}_{Rd} - \mathbf{x}_R) + \mathbf{f}_R}_{\text{injecting relative impedance behaviors}} + \underbrace{\mathbf{\Gamma}\left(\dot{\mathbf{x}}_{R,\text{ideal}} - \dot{\mathbf{x}}_R\right)}_{\text{ideal velocity feedback}} \tag{10}$$

where $\mathbf{\Gamma} \in \mathbb{R}^{n_R \times n_R}$ denotes the IVF gain and is a constant diagonal matrix and $\dot{\mathbf{x}}_{R,\text{ideal}}$, called ideal velocity, is defined as

$$\dot{\mathbf{x}}_{R,\text{ideal}} \triangleq \int \left\{\ddot{\mathbf{x}}_{Rd} + \mathbf{M}_{Rd}^{-1}\left[\mathbf{B}_{Rd}(\dot{\mathbf{x}} - \dot{\mathbf{x}}) + \mathbf{K}_{Rd}(\mathbf{x}_{Rd} - \mathbf{x}_R) + \mathbf{f}_R\right]\right\} dt. \tag{11}$$

Finally, the control torque is obtained as (12), shown at the bottom of the page.

We apply the control torque (12) to the robot dynamics (7), where $\ddot{\mathbf{q}} = \mathbf{J}_R^{+}(\ddot{\mathbf{x}}_R - \dot{\mathbf{J}}\dot{\mathbf{q}})$ and results in

$$\begin{aligned}\bar{\mathbf{M}}\mathbf{J}_R^{+}(\ddot{\mathbf{x}}_R - \dot{\mathbf{J}}\dot{\mathbf{q}}) + \mathbf{h}(\mathbf{q}, \dot{\mathbf{q}}, \ddot{\mathbf{q}}) &= \boldsymbol{\tau}_{u(t-L)} - \bar{\mathbf{M}}\ddot{\mathbf{q}}_{(t-L)} \\ &+ \bar{\mathbf{M}}\mathbf{J}_R^{+}\left\{\ddot{\mathbf{x}}_{Rd} + \mathbf{M}_{Rd}^{-1}\left[\mathbf{B}_{Rd}(\dot{\mathbf{x}}_{Rd} - \dot{\mathbf{x}}_R) + \mathbf{K}_{Rd}(\mathbf{x}_{Rd} - \mathbf{x}_R) + \mathbf{f}_R\right] - \dot{\mathbf{J}}_{\mathbf{R}}\dot{\mathbf{q}}\right\} \\ &+ \bar{\mathbf{M}}\mathbf{J}_R^{+}\mathbf{\Gamma}(\dot{\mathbf{x}}_{R,\text{ideal}} - \dot{\mathbf{x}}_R).\end{aligned} \tag{13}$$

Due to discontinuous nonlinearities, the TDE compensation cannot accurately cancel the effects of the robot dynamics, i.e.,

$$\mathbf{h}(\mathbf{q}, \dot{\mathbf{q}}, \ddot{\mathbf{q}}) \neq \hat{\mathbf{h}}(\mathbf{q}, \dot{\mathbf{q}}, \ddot{\mathbf{q}}) = \boldsymbol{\tau}_{u(t-L)} - \bar{\mathbf{M}}\ddot{\mathbf{q}}_{(t-l)}. \tag{14}$$

(This discussion can be found in [49].) Thus, the difference between the TDE compensation and discontinuous nonlinearities results into an $\boldsymbol{\epsilon}$ error

$$\epsilon = \mathbf{J}_R\bar{\mathbf{M}}^{-1}\left(\boldsymbol{\tau}_{u(t-L)} - \bar{\mathbf{M}}\ddot{\mathbf{q}}_{(t-L)} - \mathbf{h}(\mathbf{q}, \dot{\mathbf{q}}, \ddot{\mathbf{q}})\right). \tag{15}$$

Moreover, by applying (15) to (13), we obtain

$$\begin{aligned}\dot{\mathbf{x}}_R - \dot{\mathbf{x}}_{Rd} + \mathbf{M}_{Rd}^{-1}\left[\mathbf{B}_{Rd}(\dot{\mathbf{x}}_R - \dot{\mathbf{x}}_{Rd}) + \mathbf{K}_{Rd}(\mathbf{x}_R - \mathbf{x}_{Rd}) - \mathbf{f}_R\right] \\ = \epsilon - \mathbf{\Gamma}\left(\dot{\mathbf{x}}_R - \dot{\mathbf{x}}_{R,\text{ideal}}\right) = \delta\end{aligned} \tag{16}$$

where $\boldsymbol{\delta}$ represents a very small number. We tune the value of $\mathbf{\Gamma}$ by trial and error in order to keep $\boldsymbol{\epsilon} \simeq \mathbf{\Gamma}(\dot{\mathbf{x}}_R - \dot{\mathbf{x}}_{R,\text{ideal}})$. This results to our target dynamics in (6). The implementation details of this proposed controller are discussed in Section III-C.

$$\boldsymbol{\tau}_u = \underbrace{\boldsymbol{\tau}_{u(t-L)} - \bar{\mathbf{M}}\ddot{\mathbf{q}}_{(t-L)}}_{\text{time delay estimation}} + \bar{\mathbf{M}}\mathbf{J}_R^{+}\underbrace{\left\{\ddot{\mathbf{x}}_{Rd} + \mathbf{M}_{Rd}^{-1}\left[\mathbf{B}_{Rd}(\dot{\mathbf{x}}_{Rd} - \dot{\mathbf{x}}_R) + \mathbf{K}_{Rd}(\mathbf{x}_{Rd} - \mathbf{x}_R) + \mathbf{f}_R\right] - \mathbf{J}_R\dot{\mathbf{q}}\right\}}_{\text{injecting relative impedance behaviors}} + \bar{\mathbf{M}}\mathbf{J}_R^{+}\mathbf{\Gamma}\underbrace{\left(\dot{\mathbf{x}}_{R,\text{ideal}} - \dot{\mathbf{x}}_R\right)}_{\text{ideal velocity feedback}} \tag{12}$$

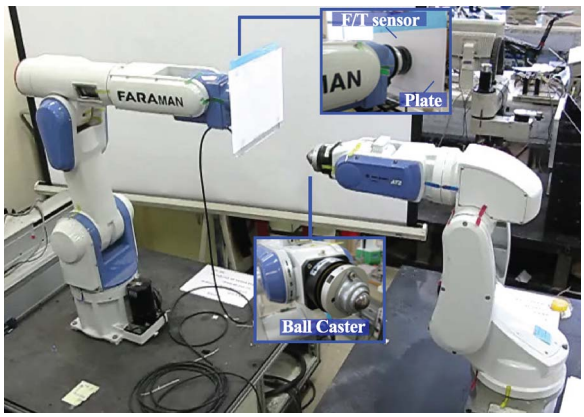

Fig. 2. Experimental setup of dual-arm system. (Left) Faraman-AC2 as a reference robot with the acrylic plate and (right) Faraman-AT2 as a tool robot with a ball caster.

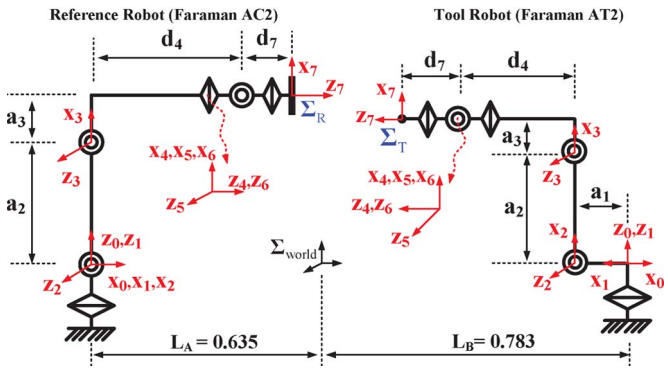

Fig. 3. Assignment of link frames for the dual-arm robot system.

TABLE I
D–H PARAMETERS OF TWO INDUSTRIAL ROBOTS. (a) FARAMAN AC2 (REFERENCE ROBOT). (b) FARAMAN AT2 (TOOL ROBOT)

(a)

i	α_{i-1}	a_{i-1}	d_{i-1}	θ_i
1	0	0	0	q_1
2	$\pi/2$	0	0	$q_2 + \pi/2$
3	0	0.42	0	q_3
4	$\pi/2$	0.1	0.5	q_4
5	$-\pi/2$	0	0	q_5
6	$\pi/2$	0	0	q_6
7	$\pi/2$	0	0.179	0

(b)

i	α_{i-1}	a_{i-1}	d_{i-1}	θ_i
1	0	0	0	$q_7 + \pi$
2	0	0	0	$q_8 - \pi/2$
3	0	0.255	0	q_9
4	$-\pi/2$	0.096	0.3	q_{10}
5	$\pi/2$	0	0	q_{11}
6	$-\pi/2$	0	0	q_{12}
7	0	0	0.151	0

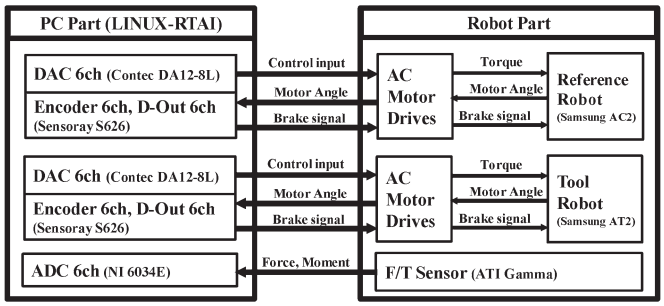

Fig. 4. Schematic diagram of the dual-arm real-time control platform.

III. EXPERIMENT

This work will present three sets of experiments to verify the proposed relative impedance control on a dual-arm system performing ABTs, including contact, noncontact, and transition, in an effective and stable manner. For a given task, this work will demonstrate how the desired trajectory and impedance can be specified.

A. Experimental Setup

A dual-arm real-time control platform is developed for the experiments.

1) Hardware Configuration: As shown in Fig. 2, the dual arm consists of two 6-DOF PUMA-type industrial robots manufactured by Samsung Corporation: Faraman-AC2 as a reference robot (left) and Faraman-AT2 as a tool robot (right). At the end effector of the reference robot, a force–torque sensor is attached, and on top of it, an acrylic plate is securely fixed. This force–torque sensor measures $\mathbf{f}_R$, i.e., the relative contact force with respect to Σ_R. The plate is covered with a sheet of white paper to make the writing more visible. A steel ball caster with red ink is attached to the end effector of the tool robot.

The frame assignment of each manipulator is shown in Fig. 3, while Table I is expressed using Denavit–Hartenberg (D–H) parameters in Craig's notation [55]. Gear reduction ratios are {207.7, 320.0, 220.0, 272.7, 138.5, 133.3} for Faraman AC2 and {120, 120, 120, 100, 80, 50} for Faraman AT2. Voltage-to-torque ratios are {87.09, 68.27, 46.93, 29.09, 7.38, 7.11} N · m/V for Faraman-AC2 and {25.45, 25.45, 12.75, 10.62, 4.26, 2.66} N · m/V for Faraman-AT2. The encoder for each joint of the two manipulators has a resolution of 2048 pulses/rev. The ATI Gamma SI-130-10 force–torque sensor has 1/80-N resolution for the forces and 1/3200-N · m resolution for the torques.

The controller uses an industrial PC with a 2.4-GHz Pentium 4 where three types of data acquisition boards are placed (as shown in Fig. 4): Two Contec DA12-8L boards output analog voltages for control inputs, two Sensoray S626 boards read joint angles and output digital signals for joint brakes, and one National Instruments PCI-6034E board obtains the data from the force–torque sensor.

2) Software Configuration: The controller is implemented by using C++ running under Linux with real-time application interface [56]. The sampling period is set to 2 ms. This system uses an open-source Linux driver COMEDI for the real-time data acquisition and an open-source library Newmat 11 for the matrix computation.

3) Contact Environment: An acrylic plate (250 mm × 250 mm × 8 mm) of light and stiff material is used.[1] The mass of the plate is 0.573 kg, and the stiffness is about 8000 N/m.

[1]It is known that a manipulator's contact task is more difficult to conduct in a stiff environment than in a soft environment [55], [57].

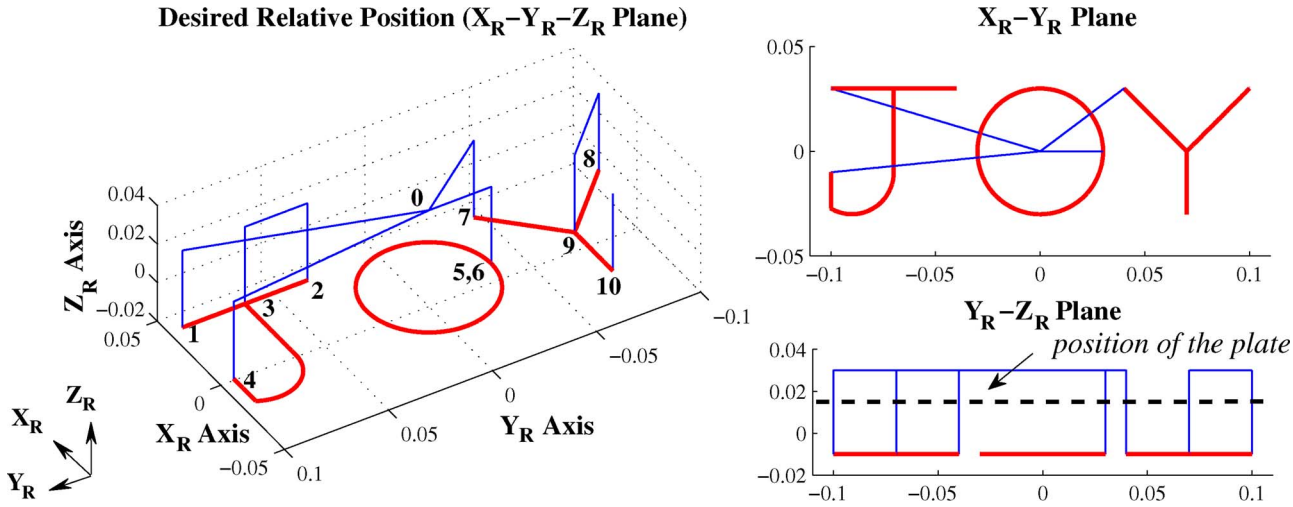

Fig. 5. Figure shows a desired relative position path $[X_R, Y_R, Z_R]^{\mathrm{T}}$. The blue solid line denotes the path of free motion, and the red solid line denotes the path of constrained motion. In the 3-D plot, the numbers from 0 to 10 indicate the order of the transition; in the Y_R–Z_R-plane plot, the black dotted line indicates the expected position of the plate.

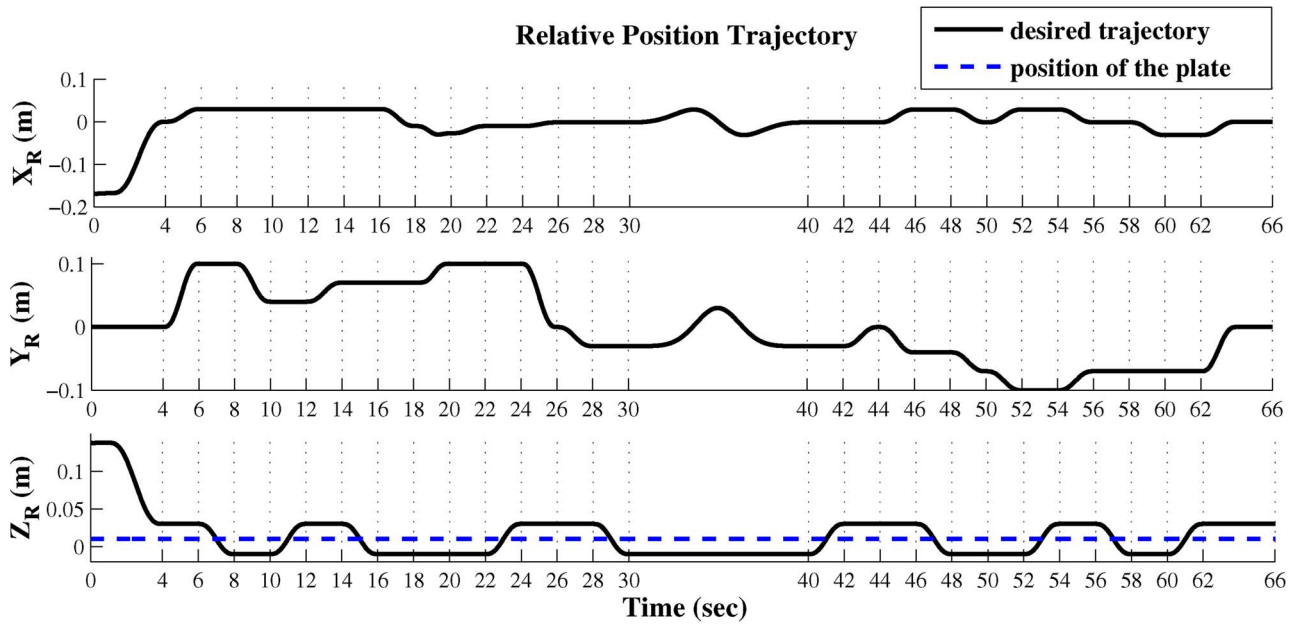

Fig. 6. Figure shows a desired relative position trajectory $[X_R(t), Y_R(t), Z_R(t)]^{\mathrm{T}}$. The grid of the time axis indicates time intervals of each segment of the trajectory. In the plot in the Z_R-axis, the (blue) dotted line indicates the expected position of the plate.

B. Description of Experiment

In order to demonstrate ABTs with contact, noncontact, and transition through coordinated action between two 6-DOF industrial robots, a writing task is conducted. The tool robot writes three letters, namely, "J," "O," and "Y," on the plate attached to the end effector of the reference robot. The details are as follows.

1) Desired Trajectories of Relative Position and Relative Orientation: The relative path $[X_R, Y_R, Z_R]^{\mathrm{T}}$ is shown in Fig. 5. It is designed to write the three-letter-word "JOY" on the X_R–Y_R plane. The displacement in the direction of the Z_R-axis is set to exceed the position of the plate in order to maintain contact during the writing. Each trajectory of the relative position is composed of 27 segments (including straight lines and curves), and each segment is formed by the fifth-order polynomial trajectory $[X_R(t), Y_R(t), Z_R(t)]^{\mathrm{T}}$ for the given time intervals, as shown in Fig. 6. Throughout the task ($t = 0$ to 66 s), the trajectories of the desired relative orientation are designed to keep the end effector of the right arm perpendicular to the plate attached to the end effector of the left arm, which makes the roll–pitch–yaw angles referenced at Σ_R equal to $[\alpha_R, \beta_R, \gamma_R]^{\mathrm{T}} = [\pi, 0, 0]^{\mathrm{T}}$, using Euler angle system II [58]. In this approach, only the desired value of $\mathbf{x}_R$ is necessary and not the individual desired values of each end effector.

2) Desired Relative Impedance: In the constrained direction Z_R of the 6-DOF task space, a compliant behavior—high damping and low stiffness—is required to perform ten transitions between the contact state and noncontact state against the stiff plate. To verify that the proposed control along Z_R can achieve the desired relative impedance precisely and robustly,

TABLE II
THREE SETS OF THE 6-DOF DESIRED RELATIVE IMPEDANCE

	$\mathbf{M}_{Rd}$	$\mathbf{B}_{Rd}$	$\mathbf{K}_{Rd}$	ζ_{Z_R}[a]
Set #1	$10 \cdot \mathbf{I}_6$[b]	$\mathrm{diag}(200, 200, 620, 200, 200, 200)$	$\mathrm{diag}(1000, 1000, 600, 1000, 1000, 1000)$	4
Set #2	$10 \cdot \mathbf{I}_6$	$\mathrm{diag}(200, 200, 700, 200, 200, 200)$	$\mathrm{diag}(1000, 1000, 500, 1000, 1000, 1000)$	5
Set #3	$10 \cdot \mathbf{I}_6$	$\mathrm{diag}(200, 200, 760, 200, 200, 200)$	$\mathrm{diag}(1000, 1000, 400, 1000, 1000, 1000)$	6

[a] ζ_{Z_R} denotes the damping ratio of the Z_R axis. The damping ratios of the other axes are all critically damped, $\zeta = 1$.
[b] $\mathbf{I}_6$ denotes the 6×6 identity matrix.

three overdamped impedance dynamics along Z_R is tested with damping ratios $\zeta_{Z_R} = 4, 5, 6$. For the remaining DOFs, a stiff behavior—low damping and high stiffness—is required for accurate writing at critically damped impedance $\zeta = 1$. For each overdamped ζ_{Z_R}, corresponding values of desired relative mass matrix $\mathbf{M}_{Rd}$, damping matrix $\mathbf{B}_{Rd}$, and stiffness matrix K_{Rd} are set. These are shown in Table II. Here, relative impedance with respect to the relative reference frame is specified and not the absolute impedances of each end effector. Note that the dual arm is controlled as a single manipulator; thus, the matrices are of size 6×6.

C. Implementation of the Proposed Controller

In order to accomplish the desired relative trajectory and relative impedance behavior, the proposed controller, as shown in (12), is used for the experiments. The selection of $\bar{\mathbf{M}}$ has a significant effect on the control performance and thus is worth mentioning. In principle, the best selection of $\bar{\mathbf{M}}$ is perhaps $\mathbf{M}(\mathbf{q})$, the actual inertia matrix. Nevertheless, since $\mathbf{M}(\mathbf{q})$ is difficult to accurately estimate and computationally demanding to implement on real-time basis, $\bar{\mathbf{M}}$ is often tuned by trial and error. More specifically, its diagonal elements are gradually increased from a small positive value within the region of stability, without using system parameters [49]. The elements of the IVF gain $\mathbf{\Gamma}$ are set at the highest values where no control chatter occurs. The closed-loop stability analysis due to this control is given in the Appendix.

Incidentally, we take note that the proposed control requires the joint acceleration $\ddot{\mathbf{q}}_{(t-L)}$ for the TDE. The encoder signal is usually contaminated by noise in the real experiment, and the effect of the noise is amplified due to the calculation of the joint acceleration by numerical differentiation. Fortunately, it was proven in [43] that the noise can be attenuated by *lowering* $\bar{\mathbf{M}}$ without explicitly using an additional low-pass filter, which has the implication of the aforementioned tuning process of $\bar{\mathbf{M}}$.

The use of our relative impedance equation, as shown in (6), results in the specification of our desired task that is equivalent to that of a single manipulator. The values of the parameters of the control law are assigned as follows. The gain $\bar{\mathbf{M}} \in \mathbb{R}^{12\times12}$ is set to $\mathrm{diag}(6.62, 5.15, 1.90, 0.84, 0.17, 0.14, 0.99, 0.97, 0.45, 0.32, 0.05, 0.02)$ kg $\cdot$ m^2, where the first six elements correspond to the reference robot and the remaining six elements correspond to the tool robot. The relative Jacobian $\mathbf{J}_R \in \mathbb{R}^{6\times12}$ is computed based on [2]. The parameters $\mathbf{x}_{Rd}$, $\dot{\mathbf{x}}_{Rd}$, and $\ddot{\mathbf{x}}_{Rd} \in \mathbb{R}^6$ are assigned based on the desired fifth-order polynomial trajectory, as shown in Figs. 5 and 6. The values of $\mathbf{M}_{Rd}$, $\mathbf{B}_{Rd}$, and $\mathbf{K}_{Rd} \in \mathbb{R}^{6\times6}$ are based on Table II. The relative position and orientation vector $\mathbf{x}_R = [X_R, Y_R, Z_R, \alpha_R, \beta_R, \gamma_R]^{\mathrm{T}} \in \mathbb{R}^6$ is computed from forward kinematics based on $\mathbf{q} \in \mathbb{R}^{12}$ feedback. The parameter $\dot{\mathbf{x}}_R \in \mathbb{R}^6 = \mathbf{J}_R\dot{\mathbf{q}}$, where $\dot{\mathbf{q}} \in \mathbb{R}^{12}$ is computed by numerical differentiation of $\mathbf{q}$. The value of $\mathbf{f}_R \in \mathbb{R}^6$ is measured by the force–torque sensor attached at the end effector of the left arm. The value of $\dot{\mathbf{J}}_R$ is calculated by using a numerical differentiation of $\mathbf{J}_R$. The gain $\mathbf{\Gamma} \in \mathbb{R}^{6\times6}$ is set to $\mathrm{diag}\,(50, 50, 50, 50, 50, 50)$. The value of $\dot{\mathbf{x}}_{R,\mathrm{ideal}} \in \mathbb{R}^6$ is based on (11). Finally, the value of $\boldsymbol{\tau}_{u(t-L)} - \bar{\mathbf{M}}\ddot{\mathbf{q}}_{(t-L)}$ is based on the previous computation cycle, where $L = 2$ ms.

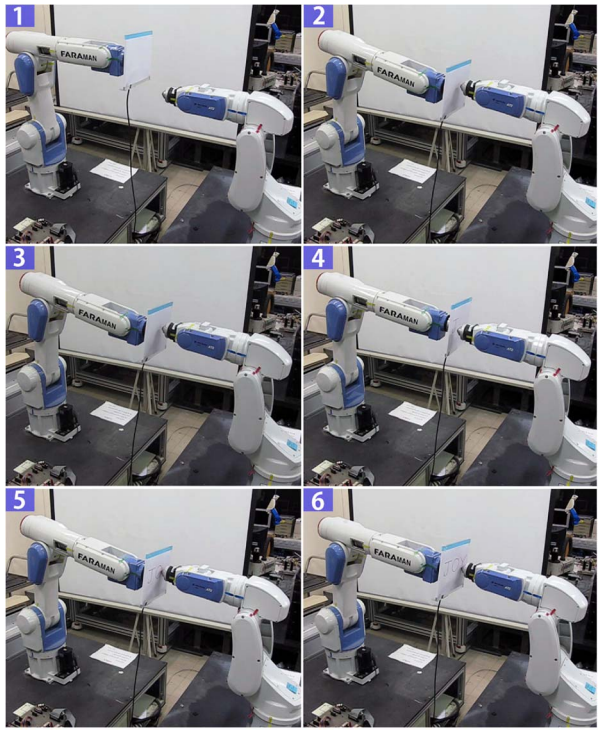

Fig. 7. Snapshots of the dual-arm system performing the writing task. The tool robot writes the word "JOY" on a plate attached to the reference robot.

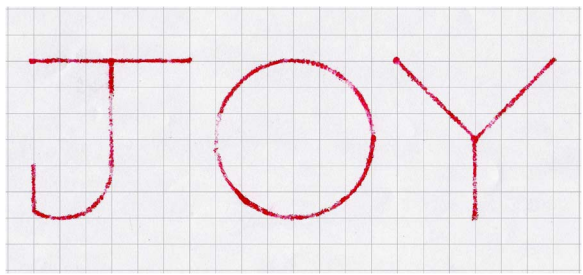

Fig. 8. Scanned image of the result of writing experiment. The length and width of the grids are 10 mm $\times$ 10 mm.

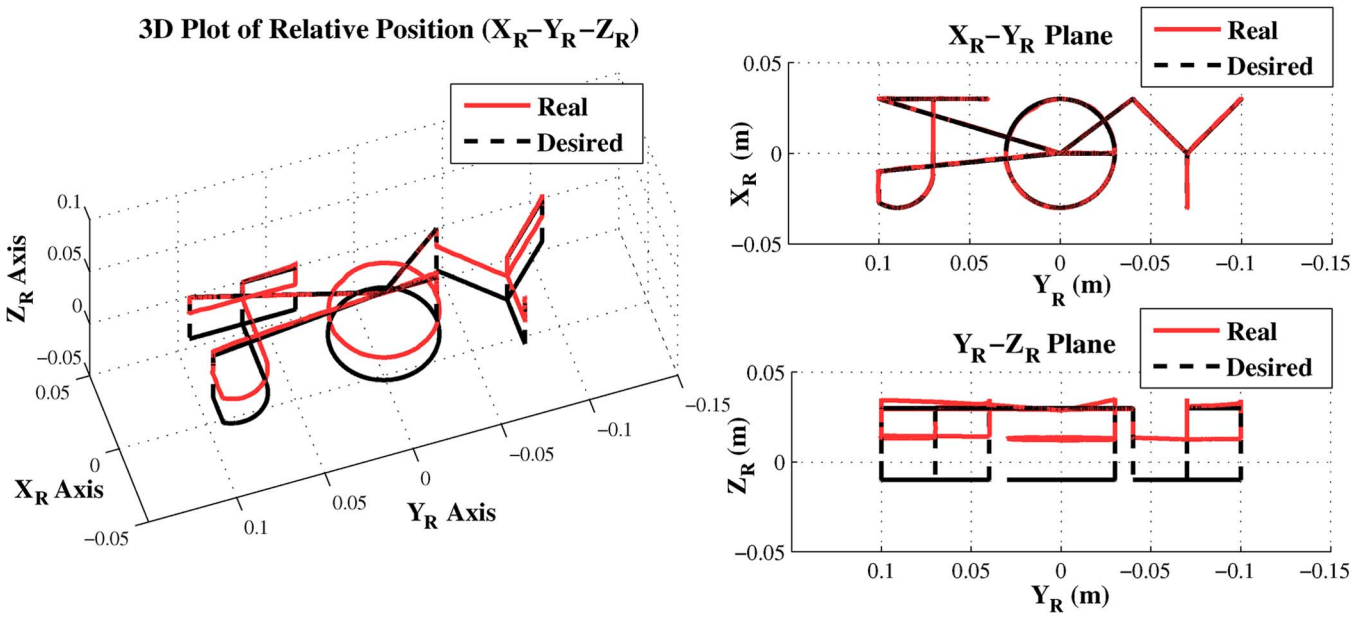

Fig. 9. Response of relative position path $[X_R, Y_R, Z_R]^{\mathrm{T}}$. The (black) dotted line indicates the desired trajectory, and the (red) solid line denotes the real trajectory.

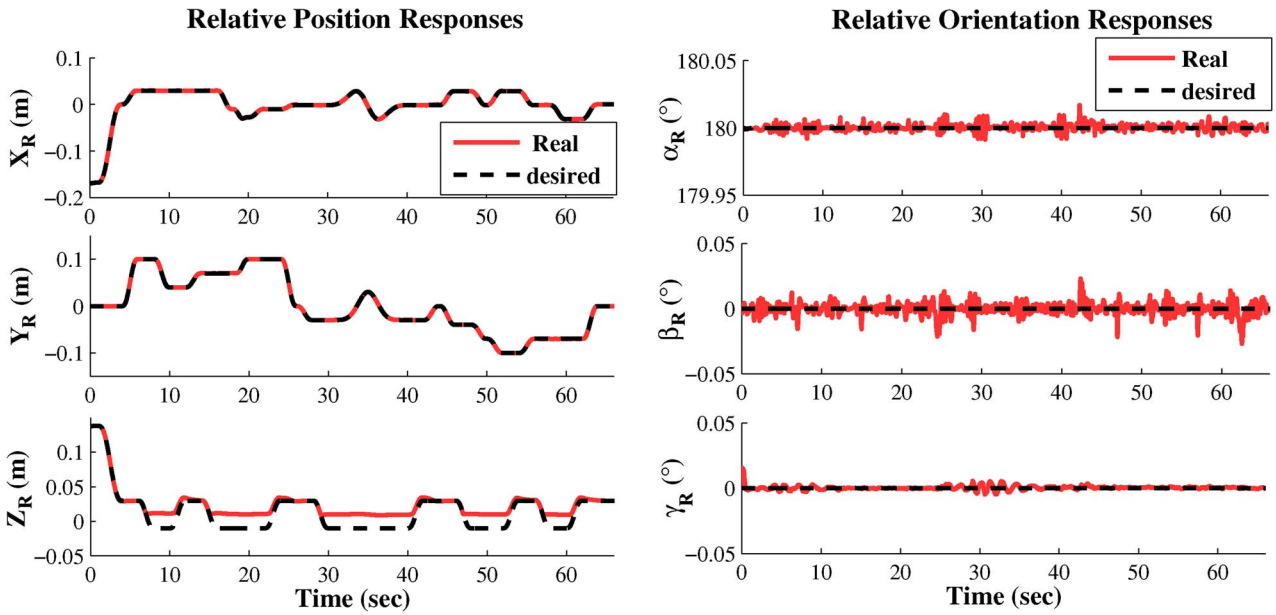

Fig. 10. Responses of relative position and orientation trajectory. The (black) dotted line indicates the desired trajectory, and the (red) solid line denotes the real trajectory.

D. Experimental Results

1) Experiment 1—Desired Relative Impedance Set #1: A dual-arm writing task is conducted with the desired impedance set #1 shown in Table II. The snapshots of the dual arm performing the desired task are shown in Fig. 7, and the experimental result is shown in Fig. 8. We can see the three-letter-word "JOY" is accurately written on the paper through the grid (10 mm × 10 mm) in the image. Note that the uneven thickness of the word turned out to be the result of irregular supply of ink to the steel ball, not the outcome of control performance. This was confirmed through the reproduction of writing with the saved data of relative position response in Fig. 9.

TABLE III
RMS ERRORS OF RELATIVE POSITION AND ORIENTATION RESPONSES

RMS error (m)		RMS error (deg)	
X_R	0.0009	α_R	0.0015
Y_R	0.0001	β_R	0.0034
Z_R	0.0160	γ_R	0.0007

The responses of relative position along the X_R-, Y_R-, and Z_R-axes in meters and relative orientation in degrees of α_R, β_R, and γ_R angles are shown in Fig. 10. The root-mean-square (rms) values of tracking errors are presented in Table III. Except for the Z_R direction, good tracking accuracy was achieved. The

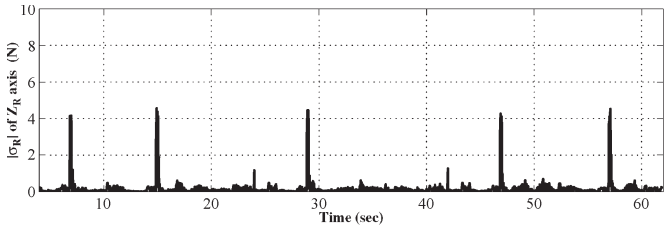

Fig. 11. Relative impedance error norm, as shown in (17), along the constrained direction Z_R.

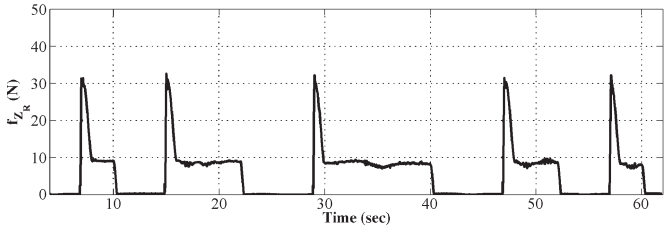

Fig. 12. Contact force response $\mathbf{f}_R$ along the constrained direction Z_R during the writing.

position error along the Z_R-direction is necessary in order to maintain contact and achieve the desired relative impedance. This result confirms that the desired relative impedance behavior is achieved well. Throughout the writing task, the value of manipulability measure for the relative Jacobian has the range $\sqrt{\det(\mathbf{J}_R\mathbf{J}_R^{\mathrm{T}})} = [3.733, 4.456]$.

In order to investigate the accuracy of the achieved relative impedance more quantitatively, we have considered the following relative impedance error norm [59]:

$$|\boldsymbol{\sigma}_R| \triangleq |(\mathbf{M}_{Rd}\ddot{\mathbf{e}}_R + \mathbf{B}_{Rd}\dot{\mathbf{e}}_R + \mathbf{K}_{Rd}\mathbf{e}_R) - \mathbf{f}_R| \qquad (17)$$

where $\mathbf{e}_R = \mathbf{x}_{Rd} - \mathbf{x}_R$ denotes the error vector of the relative position and orientation, and $\dot{\mathbf{e}}_R$ and $\ddot{\mathbf{e}}_R$ are the corresponding relative velocity and acceleration errors. The relative impedance error norm along the Z_R-direction is shown in Fig. 11. Throughout the task, the rms value of the impedance error is 0.397 N. The peaks in Fig. 11 occurred at the instance of contact with the surface and thus are construed to come from impact forces.

The correctness of $\boldsymbol{\sigma}_R$ can be verified by an inspection of the contact force response $\mathbf{f}_R$ along the $\mathbf{Z}_R$-axis shown in Fig. 12. As the response reaches the steady state, the relative impedance behavior, as shown in (6), becomes $\mathbf{f}_R \simeq \mathbf{K}_{Rd}(\mathbf{x}_{Rd} - \mathbf{x}_R)$. Therefore, an inspection of the steady state ($t = 8{-}10$, $16{-}22$, $30{-}40$, $48{-}52$, and $58{-}60$ s) reveals that the relative stiffness is 595.62 N/m, which is within about 0.73% error of the desired stiffness of 600 N/m. The peaks in the force response are due to the impact when the two end effectors come in contact. Note that the fluctuation in the steady state comes from the dynamic coupling: The force in one direction is affected by the motion of the other directions [59], [60]. From the aforementioned results, it may be concluded that the desired relative impedance is realized successfully.

2) Experiment 2—Desired Relative Impedance Sets #2 and #3: In order to verify the performance of the proposed controller when various desired impedances are implemented, the same writing task is performed under two additional conditions: the sets #2 and #3 shown in Table II. The presented variation in damping ratio is modified with respect to the damping coefficient $\mathbf{B}_{Rd}$ and spring constant $\mathbf{K}_{Rd}$. However, we can also change the damping ratio to its desired value by varying the inertia coefficient $\mathbf{M}_{Rd}$.

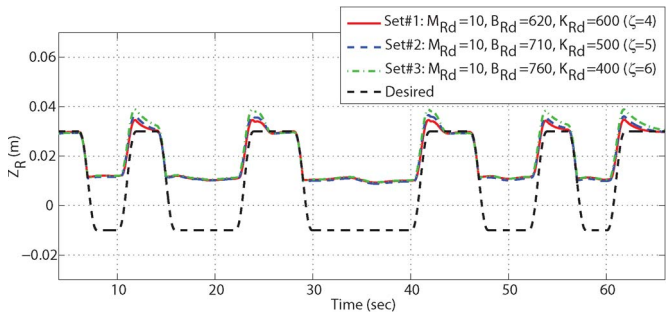

Fig. 13. Relative position response along the constrained direction Z_R as the desired relative impedance varies.

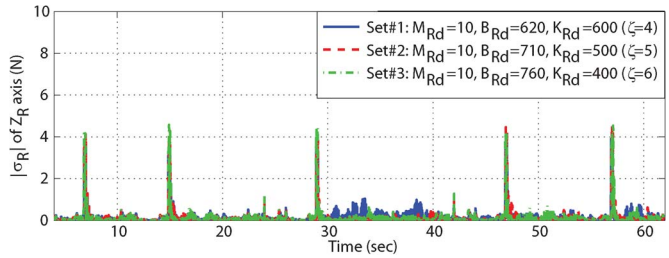

Fig. 14. Relative impedance error norm along the constrained direction Z_R during the writing task as the desired relative impedance varies.

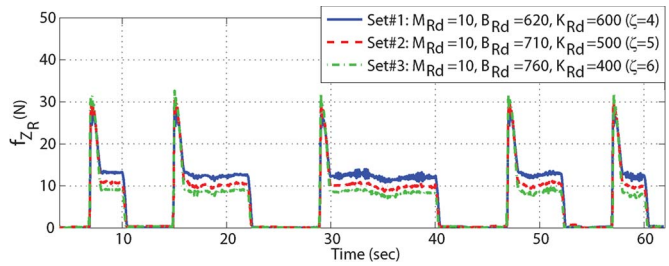

Fig. 15. Relative contact force response along the constrained direction Z_R as the desired relative impedance varies.

The relative position response along the constrained direction Z_R for the three experimental sets is shown in Fig. 13. The changes in the response according to the relative impedance are observed: The smaller the damping ratio ζ_{Z_R} of the desired relative impedance becomes, the faster is the settling time, and the smaller is the overshoot.

The relative impedance error norms along the constrained direction Z_R during the writing task for the three experiments are shown in Fig. 14: The rms errors for sets #2 and #3 are 0.419 and 0.441 N, respectively. The relative contact force responses along the constrained direction $\mathbf{f}_R$ along $\mathbf{Z}_R$ are shown in Fig. 15 with the desired stiffness of sets #1, #2, and #3. An inspection of the steady state ($t = 8{-}10$, $16{-}22$, $30{-}40$, $48{-}52$, and $58{-}60$ s) reveals that the relative stiffness values for sets #2 and #3 are very close to the desired value: The realized relative stiffness values are 505.10 and 405.4 N/m,

and their deviations from the desired values are 1.02% and 1.35%, respectively. From the aforementioned results, it can be deduced that the proposed controller achieves the desired relative impedance quite well under different impedance values.

IV. Conclusion

This work has proposed a method of implementing impedance control on a dual-arm system, which is treated as a single manipulator, and performing an ABT. The proposed task is a writing task, where the tool robot writes the word "JOY" on a plate attached to the reference robot. Through the use of a relative Jacobian, the impedance control was reduced to a single controller for both arms, such that the relative motion between the two end effectors characterized the execution of the desired task. This makes the proposed impedance control simpler and more intuitive when specifying the desired impedance and the desired trajectories. For the writing task implementation, three sets of experiments were shown at different damping ratios. The relative stiffness assumed a maximum steady-state error of 1.35%. The use of TDE made the proposed controller easier to implement. Finally, a stability analysis of the proposed controller was presented, which showed that the error was ultimately bounded.

Appendix
Stability Analysis in Section III

Here, the stability of the overall system with the control law (12) is presented. By substituting (9) into (7), the closed-loop dynamics due to the proposed control becomes

$$\bar{\mathbf{M}}\left[\mathbf{J}_R^+\left(\mathbf{v}_d-\dot{\mathbf{J}}_R\dot{\mathbf{q}}\right)-\ddot{\mathbf{q}}\right]=\mathbf{h}(\mathbf{q},\dot{\mathbf{q}},\ddot{\mathbf{q}})-\hat{\mathbf{h}}(\mathbf{q},\dot{\mathbf{q}},\ddot{\mathbf{q}}). \quad (18)$$

If $\mathbf{J}_R$ is nonsingular, the closed-loop dynamics shown in (18) can be expressed as

$$\mathbf{v}_d-\dot{\mathbf{x}}_R=\mathbf{J}_R\boldsymbol{\varepsilon} \quad (19)$$

with the TDE error $\boldsymbol{\varepsilon}$ defined as

$$\boldsymbol{\varepsilon}\triangleq\bar{\mathbf{M}}^{-1}\left[\mathbf{h}(\mathbf{q},\dot{\mathbf{q}},\ddot{\mathbf{q}})-\hat{\mathbf{h}}(\mathbf{q},\dot{\mathbf{q}},\ddot{\mathbf{q}})\right] \quad (20)$$

or by expressing $\mathbf{v}_d$ from (10)

$$\ddot{\mathbf{x}}_{Rd}-\ddot{\mathbf{x}}_R+\mathbf{M}_{Rd}^{-1}\left[\mathbf{B}_{Rd}(\dot{\mathbf{x}}_{Rd}-\dot{\mathbf{x}}_R)+\mathbf{K}_{Rd}(\mathbf{x}_{Rd}-\mathbf{x}_R)+\mathbf{f}_R\right]+\boldsymbol{\Gamma}(\dot{\mathbf{x}}_{R,\mathrm{ideal}}-\dot{\mathbf{x}}_R)=\mathbf{J}_R\boldsymbol{\varepsilon}. \quad (21)$$

Here, by defining the integral sliding surface [61] as

$$\mathbf{s}=\int\left\{\ddot{\mathbf{x}}_{Rd}-\ddot{\mathbf{x}}_R+\mathbf{M}_{Rd}^{-1}\left[\mathbf{B}_{Rd}(\dot{\mathbf{x}}_{Rd}-\dot{\mathbf{x}}_R)+\mathbf{K}_{Rd}(\mathbf{x}_{Rd}-\mathbf{x}_R)+\mathbf{f}_R\right]\right\}dt \quad (22)$$

and from (11), we get $\mathbf{s}=\dot{\mathbf{x}}_{R,\mathrm{ideal}}-\dot{\mathbf{x}}_R$; the closed-loop dynamics can be obtained as follows:

$$\dot{\mathbf{s}}+\boldsymbol{\Gamma}\mathbf{s}=\mathbf{J}_R\boldsymbol{\varepsilon}. \quad (23)$$

If $\mathbf{J}_R\boldsymbol{\varepsilon}$ is asymptotically bounded, then the overall system is bounded-input–bounded-output stable. Therefore, to prove the stability, we investigate the following inequality equation:

$$\|\dot{\mathbf{s}}+\boldsymbol{\Gamma}\mathbf{s}\|=\|\mathbf{J}_R\boldsymbol{\varepsilon}\|\le\|\mathbf{J}_R\|\,\|\boldsymbol{\varepsilon}\|. \quad (24)$$

From the definition of the relative Jacobian, $\dot{\mathbf{x}}_R=\mathbf{J}_R\dot{\mathbf{q}}$, it can be inferred that, if $\mathbf{J}_R$ is unbounded, then even very small joint displacement causes infinite displacement of relative position (or orientation); however, it will never happen in the physical system. Hence, the relative Jacobian is bounded as

$$\|\mathbf{J}_R\|\le\alpha \quad (25)$$

where α has a positive value. To find the boundedness of $\boldsymbol{\varepsilon}$, by defining the reference joint acceleration as $\ddot{\mathbf{q}}^*\triangleq\mathbf{J}_R^+(\mathbf{v}_d-\dot{\mathbf{J}}_R\dot{\mathbf{q}})$, (18) can be reformulated as follows:

$$\ddot{\mathbf{q}}^*-\ddot{\mathbf{q}}=\boldsymbol{\varepsilon}. \quad (26)$$

According to the proof provided in [49] and [62], if the time delay L is sufficiently small and the roots of $[\mathbf{I}-\mathbf{M}^{-1}\bar{\mathbf{M}}]$ reside inside a unit circle, the TDE error $\boldsymbol{\varepsilon}$ is bounded as

$$\|\boldsymbol{\varepsilon}\|\le\beta \quad (27)$$

where β has a positive value. From (24), (25), and (27), it can be determined that

$$\|\dot{\mathbf{s}}+\boldsymbol{\Gamma}\mathbf{s}\|=\|\mathbf{J}_R\boldsymbol{\varepsilon}\|\le\alpha\beta\triangleq\gamma \quad (28)$$

where γ has a positive value.

Then, Lyapunov-based stability of the overall system can be proven in the same manner as the stability proof in [49]. The Lyapunov function can be taken as $V=0.5\mathbf{s}^{\mathrm{T}}\mathbf{s}$; the derivative of V is given by $\dot{V}=-\mathbf{s}\boldsymbol{\Gamma}\mathbf{s}+\mathbf{s}^{\mathrm{T}}\mathbf{J}_R\boldsymbol{\varepsilon}$. Then, we can obtain $\dot{V}<0$ under the condition $|\mathbf{s}_i|>|\{\boldsymbol{\Gamma}^{-1}\mathbf{J}_R\boldsymbol{\varepsilon}\}_i|$, where the subscript $\bullet_i$ denotes the ith element of the vector $\bullet$. Since $\mathbf{J}_R\boldsymbol{\varepsilon}$ is bounded as (28), the integral sliding surface $\mathbf{s}$ is globally uniformly ultimately bounded with the ultimate bound $|\mathbf{s}_i|\le\gamma\|\boldsymbol{\Gamma}^{-1}\|$.

References

[1] C. Lewis and A. Maciejewski, "Trajectory generation for cooperating robots," in *Proc. IEEE Int. Conf. Syst. Eng.*, Aug. 1990, pp. 300–303.

[2] A. Mohri, M. Yamamoto, and G. Hirano, "Cooperative path planning for two manipulators," in *Proc. IEEE Int. Conf. Robot. Autom.*, 1996, vol. 3, pp. 2853–2858.

[3] T. Hsia, T. Lasky, and Z. Guo, "Robust independent joint controller design for industrial robot manipulators," *IEEE Trans. Ind. Electron.*, vol. 38, no. 1, pp. 21–25, Feb. 1991.

[4] K. Youcef-Toumi and O. Ito, "A time delay controller for systems with unknown dynamics," *J. Dyn. Syst., Meas. Control*, vol. 112, no. 1, pp. 133–142, Mar. 1990.

[5] Y. Jin, P. Chang, M. Jin, and D. Gweon, "Stability guaranteed time delay control of manipulators using nonlinear damping and terminal sliding mode," *IEEE Trans. Ind. Electron.*, vol. 60, no. 8, pp. 3304–3317, Aug. 2013.

[6] J. Lee, M. Jin, and K. K. Ahn, "Precise tracking control of shape memory alloy actuator systems using hyperbolic tangential sliding mode control with time delay estimation," *Mechatronics*, vol. 23, no. 3, pp. 310–317, Apr. 2013.

[7] N. Hogan, "Impedance control: An approach to manipulation: Part 1," *J. Dyn. Syst., Meas. Control*, vol. 107, no. 1, pp. 1–7, Mar. 1985.

[8] N. Hogan, "Impedance control: An approach to manipulation: Part 2," *J. Dyn. Syst., Meas. Control*, vol. 107, no. 1, pp. 8–16, Mar. 1985.

[9] N. Hogan, "Impedance control: An approach to manipulation: Part 3," *J. Dyn. Syst., Meas. Control*, vol. 107, no. 1, pp. 17–24, Mar. 1985.

[10] S. Schneider and R. Cannon, Jr., "Object impedance control for cooperative manipulation: Theory and experimental results," *IEEE Trans. Robot. Autom.*, vol. 8, no. 3, pp. 383–394, Jun. 1992.

[11] R. Bonitz and T. Hsia, "Internal force-based impedance control for cooperating manipulators," *IEEE Trans. Robot. Autom.*, vol. 12, no. 1, pp. 78–89, Feb. 1996.

[12] F. Caccavale, P. Chiacchio, A. Marino, and L. Villani, "Six-DOF impedance control of dual-arm cooperative manipulators," *IEEE/ASME Trans. Mechatronics*, vol. 13, no. 5, pp. 576–586, Oct. 2008.

[13] Y. Guiard, "Asymmetric division of labor in human skilled bimanual action: The kinematic chain as a model," *J. Motor Behav.*, vol. 19, no. 4, pp. 486–517, Dec. 1987.

[14] R. Zollner, T. Asfour, and R. Dillmann, "Programming by demonstration: Dual-arm manipulation tasks for humanoid robots," in *Proc. IEEE/RSJ Int. Conf. IROS*, 2004, vol. 1, pp. 479–484.

[15] M. Uchiyama and P. Dauchez, "A symmetric hybrid position/force control scheme for the coordination of two robots," in *Proc. IEEE Int. Conf. Robot. Autom.*, 1988, pp. 350–356.

[16] T. Yoshikawa and X. Zheng, "Coordinated dynamic hybrid position/force control for multiple robot manipulators handling one constrained object," *Int. J. Robot. Res.*, vol. 12, no. 3, pp. 219–230, Jun. 1993.

[17] A. Albu-Schaffer, O. Eiberger, M. Grebenstein, S. Haddadin, C. Ott, T. Wimbock, S. Wolf, and G. Hirzinger, "Soft robotics," *IEEE Robot. Autom. Mag.*, vol. 15, no. 3, pp. 20–30, Sep. 2008.

[18] T. Osone, J. Tatsuno, T. Nishida, and H. Kobayashi, "Cooperative motion planning for dual arm robot to demonstrate human arm movements," in *Proc. 11th IEEE Int. Workshop Robot Human Interact. Commun.*, 2002, pp. 488–493.

[19] F. Caccavale, C. Natale, B. Siciliano, and L. Villani, "Control of two industrial robots for parts mating," in *Proc. IEEE Int. Conf. Control Appl.*, 1998, vol. 1, pp. 562–566.

[20] F. Caccavale, C. Natale, B. Siciliano, and L. Villani, "Achieving a cooperative behavior in a dual-arm robot system via a modular control structure," *J. Robot. Syst.*, vol. 18, no. 12, pp. 691–699, Dec. 2001.

[21] T. Wimböck, C. Ott, and G. Hirzinger, "Impedance behaviors for two-handed manipulation: Design and experiments," in *Proc. IEEE Int. Conf. IEEE Robot. Autom.*, 2007, pp. 4182–4189.

[22] O. Donchin, A. Gribova, O. Steinberg, H. Bergman, and E. Vaadia, "Primary motor cortex is involved in bimanual coordination," *Nature*, vol. 395, no. 6699, pp. 274–278, Sep. 1998.

[23] F. G. Andres, T. Mima, A. E. Schulman, J. Dichgans, M. Hallett, and C. Gerloff, "Functional coupling of human cortical sensorimotor areas during bimanual skill acquisition," *Brain*, vol. 122, no. 5, pp. 855–870, May 1999.

[24] H. Wu, L. Lou, C.-C. Chen, S. Hirche, and K. Kuhnlenz, "Cloud-based networked visual servo control," *IEEE Trans. Ind. Electron.*, vol. 60, no. 2, pp. 554–566, Feb. 2013.

[25] Z. Wang and D. Gu, "Cooperative target tracking control of multiple robots," *IEEE Trans. Ind. Electron.*, vol. 59, no. 8, pp. 3232–3240, Aug. 2012.

[26] O. Linda and M. Manic, "Fuzzy force-feedback augmentation for manual control of multirobot system," *IEEE Trans. Ind. Electron.*, vol. 58, no. 8, pp. 3213–3220, Aug. 2011.

[27] S. Yang, A. Zhu, G. Yuan, and M. Meng, "A bioinspired neurodynamics-based approach to tracking control of mobile robots," *IEEE Trans. Ind. Electron.*, vol. 59, no. 8, pp. 3211–3220, Aug. 2012.

[28] S. Rahman, R. Ikeura, S. Hayakawa, and H. Sawai, "Design and control of a power assist system for lifting objects based on human operator's weight perception and load force characteristics," *IEEE Trans. Ind. Electron.*, vol. 58, no. 8, pp. 3141–3150, Aug. 2011.

[29] W. Xu, J.-S. Pap, and J. Bronlund, "Design of a biologically inspired parallel robot for foods chewing," *IEEE Trans. Ind. Electron.*, vol. 55, no. 2, pp. 832–841, Feb. 2008.

[30] J. Yuan, G. Liu, and B. Wu, "Power efficiency estimation-based health monitoring and fault detection of modular and reconfigurable robot," *IEEE Trans. Ind. Electron.*, vol. 58, no. 10, pp. 4880–4887, Oct. 2011.

[31] O. Linda and M. Manic, "Self-organizing fuzzy haptic teleoperation of mobile robot using sparse sonar data," *IEEE Trans. Ind. Electron.*, vol. 58, no. 8, pp. 3187–3195, Aug. 2011.

[32] T. Shibata and T. Murakami, "Power-assist control of pushing task by repulsive compliance control in electric wheelchair," *IEEE Trans. Ind. Electron.*, vol. 59, no. 1, pp. 511–520, Jan. 2012.

[33] B. Cai and Y. Zhang, "Different-level redundancy-resolution and its equivalent relationship analysis for robot manipulators using gradient-descent and Zhang's neural-dynamic methods," *IEEE Trans. Ind. Electron.*, vol. 59, no. 8, pp. 3146–3155, Aug. 2012.

[34] M. Shahbazi, P. Poure, S. Saadate, and M. Zolghadri, "Fault-tolerant five-leg converter topology with FPGA-based reconfigurable control," *IEEE Trans. Ind. Electron.*, vol. 60, no. 6, pp. 2284–2294, Jun. 2013.

[35] J. Jin, S. Yuen, Y. Lee, C. Jun, Y. Kim, S. Lee, B.-J. You, and N. Doh, "Minimal grasper: A practical robotic grasper with robust performance for pick-and-place tasks," *IEEE Trans. Ind. Electron.*, vol. 60, no. 9, pp. 3796–3805, Sep. 2013.

[36] C. Westermayer, R. Priesner, M. Kozek, and R. Bauer, "High dynamic torque control for industrial engine test beds," *IEEE Trans. Ind. Electron.*, vol. 60, no. 9, pp. 3877–3888, Sep. 2013.

[37] Y. Maeda and M. Iwasaki, "Initial friction compensation using rheology-based rolling friction model in fast and precise positioning," *IEEE Trans. Ind. Electron.*, vol. 60, no. 9, pp. 3865–3876, Sep. 2013.

[38] J. Lee, S. Han, and J. Lee, "Decoupled dynamic control for pitch and roll axes of the unicycle robot," *IEEE Trans. Ind. Electron.*, vol. 60, no. 9, pp. 3814–3822, Sep. 2013.

[39] C. Mitsantisuk, S. Katsura, and K. Ohishi, "Force control of human–robot interaction using twin direct-drive motor system based on modal space design," *IEEE Trans. Ind. Electron.*, vol. 57, no. 4, pp. 1383–1392, Apr. 2010.

[40] W.-H. Zhu and J. De Schutter, "Control of two industrial manipulators rigidly holding an egg," *IEEE Control Syst.*, vol. 19, no. 2, pp. 24–30, Apr. 1999.

[41] J. Szewczyk, F. Plumet, and P. Bidaud, "Planning and controlling cooperating robots through distributed impedance," *J. Robot. Syst.*, vol. 19, no. 6, pp. 283–297, Jun. 2002.

[42] J. D. Choi, "Robot and method of controlling cooperative work thereof," U.S. Patent 2009/0287 354 A1, Nov. 19, 2009.

[43] P. Chang, D. Kim, and K. Park, "Robust force/position control of a robot manipulator using time-delay control," *Control Eng. Pract.*, vol. 3, no. 9, pp. 1255–1264, Sep. 1995.

[44] A. Ejiri, I. Watanabe, K. Okabayashi, M. Hashima, M. Tatewaki, T. Aoki, and T. Maruyama, "Satellite berthing experiment with a two-armed space robot," in *Proc. IEEE Int. Conf. Robot. Autom.*, May 1994, pp. 3480–3487.

[45] K. Saiki, A. S. R. Liza, S. Toritani, and K. Nonami, "Force sensorless impedance control of dual-arm manipulator-hand system," *J. Syst. Des. Dyn.*, vol. 5, no. 5, pp. 953–965, 2011.

[46] K.-K. Ahn and S.-Y. Yang, "Robust force control of a 6 link electrohydraulic manipulator," in *Proc. 4th Korea-Russia Int. Symp. Sci. Technol. KORUS*, 2000, vol. 3, pp. 78–83.

[47] K. Ahn and S. Yokota, "Robust force control of a 6-link electro-hydraulic manipulator," *JSME Int. J. Ser. C Mech. Syst., Mach. Elements Manuf.*, vol. 46, no. 3, pp. 1091–1099, 2003.

[48] K. K. Ahn and S. Yokota, "Design of a robust force control system for an automatic live-line maintenance robot using a force disturbance observer," *Proc. Inst. Mech. Eng., Part I, J. Syst. Control Eng.*, vol. 218, no. 7, pp. 545–556, Oct. 2004.

[49] M. Jin, S. Kang, and P. Chang, "Robust compliant motion control of robot with nonlinear friction using time-delay estimation," *IEEE Trans. Ind. Electron.*, vol. 55, no. 1, pp. 258–269, Jan. 2008.

[50] B. Cao, G. Dodds, and G. Irwin, "Redundancy resolution and obstacle avoidance for cooperative industrial robots," *J. Robot. Syst.*, vol. 16, no. 7, pp. 405–417, Jul. 1999.

[51] W. Owen, E. Croft, and B. Benhabib, "Stiffness optimization for two-armed robotic sculpting," *Ind. Robot, Int. J.*, vol. 35, no. 1, pp. 46–57, 2008.

[52] B. Siciliano, L. Sciavicco, L. Villani, and G. Oriolo, *Robotics: Modelling, Planning and Control*. New York, NY, USA: Springer-Verlag, 2008.

[53] W. Newman, "Stability and performance limits of interaction controllers," *J. Dyn. Syst., Meas. Control*, vol. 114, no. 4, pp. 563–570, 1992.

[54] M. Dohring and W. Newman, "The passivity of natural admittance control implementations," in *Proc. IEEE ICRA*, 2003, vol. 3, pp. 3710–3715.

[55] J. Craig, *Introduction to Robotics: Mechanics and Control*, 3rd ed. Upper Saddle River, NJ, USA: Pearson Educ., 2005.

[56] L. Dozio and P. Mantegazza, "Real time distributed control systems using RTAI," in *Proc. 6th IEEE Int. Symp. Object-Oriented Real-Time Distrib. Comput.*, 2003, pp. 11–18.

[57] S. Eppinger, "Modeling robot dynamic performance for endpoint force control," Ph.D. dissertation, Dept. Mech. Eng., Massachusetts Inst. Technol., Cambridge, MA, USA, 1988.

[58] K. S. Fu, R. C. Gonzalez, and C. S. G. Lee, *Robotics: Control, Sensing, Vision, and Intelligence*. New York, NY, USA: McGraw-Hill, 1987.

[59] S. Kang, M. Jin, and P. Chang, "A solution to the accuracy/robustness dilemma in impedance control," *IEEE/ASME Trans. Mechatronics*, vol. 14, no. 3, pp. 282–294, Jun. 2009.
[60] P. Chang, B. Park, and K. Park, "An experimental study on improving hybrid position/force control of a robot using time delay control," *Mechatronics*, vol. 6, no. 8, pp. 915–931, Dec. 1996.
[61] J.-J. Slotine, "Robustness issues in robot control," in *Proc. IEEE Int. Conf. Robot. Autom.*, Mar. 1985, vol. 2, pp. 656–661.
[62] M. Jin, J. Lee, P. Chang, and C. Choi, "Practical nonsingular terminal sliding-mode control of robot manipulators for high-accuracy tracking control," *IEEE Trans. Ind. Electron.*, vol. 56, no. 9, pp. 3593–3601, Sep. 2009.

Jinoh Lee (S'09–M'13) received the B.S. degree in mechanical engineering from Hanyang University, Seoul, Korea, in 2003 and the M.Sc. and Ph.D. degrees in mechanical engineering from the Korea Advanced Institute of Science and Technology, Daejeon, Korea, in 2012.

He is currently a Postdoctoral Researcher with the Istituto Italiano di Tecnologia, Genoa, Italy, involved in European project FP7 ICT-287513, Safe and Autonomous Physical Human-Aware Robot Interaction. His research interests include dual-arm dexterous manipulation, robust control of highly nonlinear systems, and compliant robotic system control for safe human–robot interaction.

Pyung Hun Chang (S'86–M'89) received the M.Sc. and Ph.D. degrees in mechanical engineering from the Massachusetts Institute of Technology, Cambridge, MA, USA, in 1984 and 1987, respectively.

He had been a Professor with the Korea Advanced Institute of Science and Technology, Daejeon, Korea, for 24 years, and is currently a Professor and the Head of the Robotics Engineering Department, Daegu Gyeongbuk Institute of Science and Technology (DGIST), Daegu, Korea. He currently serves as the Dean of graduate student of DGIST. He has authored more than 46 papers in international journals, 22 papers in domestic journals, and 88 papers in conference proceedings. His current research interests include rehabilitation robotics, robust control of nonlinear systems including kinematically redundant manipulators, and impedance control of dual-arm manipulators.

Rodrigo S. Jamisola, Jr. (S'97–M'08) received the B.S. degree in mechanical engineering from the University of the Philippines–Diliman, Quezon City, Philippines, the M.E. degree (research based) in mechanical engineering from the National University of Singapore, Singapore, in 2001, the M.Sc. degree in electrical and computer engineering from Colorado State University, Fort Collins, CO, USA, in 2006, and the Ph.D. degree in electronics and communications engineering from De La Salle University, Manila, Philippines, in 2009.

He joined De La Salle University as an Assistant Professor in 2008 and Toyota Motor Philippines as the R&D Manager in 2011. He is currently a Postdoctoral Research Fellow with Daegu Gyeongbuk Institute of Science and Technology, Daegu, Korea. His research interests include control of combined manipulators, development of wearable robots, numerical optimization, and human–machine interfaces.